



Research Article

Preparation and Electrical Properties of Nanocomposite Based on Epoxy Resin and Core-Shell Polyaniline/Multi-Walled Carbon Nanotubes

Seyed Mohamad Reza Paran 

Center of Excellence in Electrochemistry, School of Chemistry, College of Science, University of Tehran, Tehran 1417935840, Iran
E-mail: m.paran@ippi.ac.ir

Received: 18 June 2024; **Revised:** 18 October 2024; **Accepted:** 18 October 2024

Abstract: Nanocomposites of epoxy resin containing various concentrations of carboxylated multiwalled carbon nanotubes (C-MWCNTs) and surface modified C-MWCNTs various concentration of both C-MWCNTs and core-shell nanoparticles were prepared. The physical, mechanical and electrical properties of prepared epoxy nanocomposites were investigated using experimental evaluations such as dynamic mechanical thermal analysis (DMTA), differential scanning calorimeter (DSC), and tensile strength measurements. The results of DSC tests revealed that the introduction of nanoparticles into the epoxy resin did not have much effect on the curing system, and by adding these nanoparticles to the epoxy resin, there is no need to change the curing system. However, the released energy during of epoxy curing show a 24% increase with the introduction of nanofiller into the epoxy matrix. The results of electrical conductivity measurements indicated a higher elastic dielectric constant for nanocomposites up to 200% incomparision with neat epoxy resin. The use of these epoxy nanocomposites in modern electrical and electro-optical industries is of great practical importance.

Keywords: epoxy resin, polyaniline, carboxylated carbon nanotubes, core-shell, electrical properties

1. Introduction

One of the common types of core-shell nanocomposites is the family of organic/inorganic nanocomposites, in which the nanocomposite material has both the properties and advantages of inorganic materials (such as hardness, thermal stability, etc.) and the advantages of organic materials (including flexibility, dielectric strength, toughness and processability, etc.) [1]. Therefore, the properties of the final nanocomposite are a combination of the properties of organic and inorganic materials (polymeric macromolecules) [2]. In organic/inorganic core-shell nanocomposites, the core can be made of an inorganic material and the shell of polymer macromolecules (organic material) or vice versa. These nanocomposites can be made from various types of polymers [3].

Carbon nanotubes (CNTs) are long hollow cylinders made from rolled graphite sheets [4]. CNTs have a relatively high ratio of length to diameter (about 1,000), which can be considered as one-dimensional structures [5]. The type of structure of carbon nanotubes has a significant effect on their properties. For example, properties such as electrical conductivity and density are highly dependent on the structure of nanotubes [6]. Some carbon nanotubes are non-conductive, while some are conductive and act like metals. Based on the literature review, it has been found that the diameter and structure are both effective in the conduction rate of nanotubes [7]. The larger the diameter of the

nanotube, the more similar its behavior to graphite. In small diameters, the effect of nanotube structure on its properties is greater than the effect of diameter [8]. Our previous research focused on the effect of various concentrations of CNTs on the properties of rubber nanocomposites and found that the introduction of only 0.5 wt%, caused a rise in the tensile strength and Young's modulus [9]. The effect of various concentrations of multiwalled carbon nanotubes (MWCNTs) on the elastoplastic behavior, thermal and rheological properties of compatibilized nanocomposites based on low density polyethylene was explored by using experimental and theoretical analysis [10]. The experimental analyses revealed that the MWCNTs can raise the Young's modulus of prepared nanocomposites to 63% depending on the nanotube concentration and dispersion state. Thermal decomposition investigations demonstrated a higher thermal stability up to 10 °C for nanocomposites containing 2 wt%, MWCNTs [6].

Among the different types of electrically conductive polymers, polyaniline has received special attention due to its good processability, environmental stability, and biocompatibility [11]. This polymer has very good electrical, magnetic, and optical properties, so that in the last ten years, it has attracted the attention of many researchers [12]. Polyaniline is an environmentally stable and noble polymer. It has been observed that this polymer can remain stable and not damaged in environments where even stainless steel is damaged [13]. Polyanilines can be used in electrical, optical, electro-optical and electrochemical applications [14]. In the last few years, researchers have been able to successfully use doped polyaniline in the manufacture of cell phone batteries and calculators, light emitting diode and LCD technology [15].

Epoxy resins are the thermoset polymers with an amorphous structure and high cross-links [16]. This resin is usually prepared from the reaction of epichlorohydrin (chloromethyloxirane) with a compound containing several active hydroxyl groups, mainly bisphenol A [17]. Epoxy resins have many applications in various industries due to their good mechanical properties and appropriate wear, thermal and chemical properties, as well as their insulation against electric current [18]. These resins are relatively brittle and have little resistance to crack initiation and propagation [19]. Our previously published papers in the field of epoxy nanocomposites which leads to a higher mechanical properties and thermal stability [19-22].

Epoxy/carbon nanotube composite is brittle and has high viscosity during processing [23]. Bubbles are created by increasing the viscosity when mixing hardener, epoxy and carbon nanotube [24]. High viscosity reduces degassing and bubbles remain in the matrix [25]. Initial defects due to bubbles are initiated and result in a reduction in failure strain [26]. The brittle failure of the nanocomposite is due to its rougher surface than pure epoxy. Therefore, the nanotube with a weak interface is pulled out and its mechanical properties will not change much [27]. Functionalization of nanotubes reduces the elongation of the matrix. By increasing the number of carbon nanotubes, the interpenetrated structure of carbon nanotubes leads to an increase in the aspect ratio (about 1,000) and the specific surface area, and the storage modulus increases [28]. The increase of carbon nanotubes causes the interaction between particles-particles and particles-polymer and creates networks in the matrix and leads to the creation of a cylindrical shape with a high aspect ratio. It should be noted that the mechanical properties are affected by an increase in the aspect ratio [29].

The main goals of this research are the surface modification of carboxylated multi-walled carbon nanotubes with core/shell morphology and analyzing the properties, morphology and electrical conductivity of the prepared nanocomposites. The effect of various concentrations of Polyaniline (PANI)/C-MWCNTs on the mechanical and electrical properties of epoxy resin as a widely used resin in the aviation industries was investigated and compared with the nanocomposites containing various C-MWCNTs loading. The structure of the carbon nanotube/polyaniline core shell and the physical composition of polyaniline and carbon nanotube with a weight ratio matrix on the final properties and especially the electrical conductivity at different frequencies have been studied.

2. Experimental

2.1 Materials

The raw materials used for the synthesis of polyaniline nanocomposite/carbon nanotubes with core-shell morphology and then making the synthesized nanoparticle-epoxy resin nanocomposite are as follows:

Aniline (manufactured by Merck): it has been used as a monomer for the synthesis of polyaniline. Ammonium persulfate (manufactured by Merck): it has been used as an oxidizing agent in the chemical oxidation synthesis of polyaniline. Distilled water: it has been used as the solvent used for the reaction medium and the washing solvent of the

synthesized product. Hydrochloric acid: it has been used as a doping acid for polyaniline. Methanol: it has been used as a washing solvent for synthetic products. Carboxylated multi-walled carbon nanotubes (made by Neutrino company with 95% purity): it has been used as a nanometer filler in the manufacture of core-shell nanocomposites. The resin used in this research is liquid epoxy resin with trade code LY5052, a product of Huntsman Company, USA. Hardener: it includes an amine-based hardener with the brand name HY5052 and the product of Huntsman, America, the amount of which should be 38 grams per 100 grams of resin. The reason for using the amine curing system is that due to the low density of core-shell nanoparticles when mixing nanoparticles with epoxy resin, the viscosity of the system increases greatly, which causes problems including: lack of proper mixing, inability to debubble in the production process and the impossibility of molding are suitable. The amine curing system used is liquid and has a low viscosity (40-60 cps) and good mechanical and electrical properties, low shrinkage and long service life.

2.2 Nanocomposites preparation

In the first step, by distilling aniline (at the boiling temperature of aniline about 184.1 °C), pure aniline is prepared. Then, in the second step, 0.35 grams of carboxylated carbon nanotubes are added to 100 ml of HCl solution and mixed for 5 minutes using a high shear mechanical stirrer, then 3 times each time for 1 minute under irradiation. Ultrasonication is placed until the carbon nanotubes are completely dispersed in the acidic medium, after which it is mixed again for 5 minutes using a high shear mechanical stirrer. Then the resulting mixture is added to the reaction reactor. Then 3.5 grams of pure aniline is dissolved in 200 ml of one molar HCl solution and added to the polymerization reaction reactor. We dissolve 1/4 gram of ammonium persulfate in 100 ml of distilled water. By gradually adding ammonium persulfate solution to the reaction reactor for 1 hour, the polyaniline in situ polymerization reaction starts in the presence of carbon nanotubes. The reaction reactor is placed inside a hot water bath so that the reaction takes place at a temperature between 20 and 25 °C. It should be noted that the temperature inside the reactor is constantly controlled by using a mercury thermometer. During the polymerization reaction, the reaction system is stirred by a mechanical stirrer and after a short time, the color of reaction mixture changes to dark green, which indicates the proper progress of the polymerization reaction of aniline and the formation of emeraldine salt. The polymerization reaction continued for 3 hours until the polymerization reaction was completed and a polymer with a suitable molecular mass was synthesized. In the third step, after the end of the reaction, the produced green suspension is filtered and the filtered polymer product is washed several times with distilled water and methanol. The synthesized emeraldine salt was placed in a vacuum oven at a temperature of 70 °C for 24 hours in order to completely dry. The synthesized product is then collected with the ratio of polyaniline to MWCNTs about 10:1. For the preparation of nanocomposites, 6 samples with different weight percentages were made as displayed in Table 1. All the samples are compared to the reference sample (pure epoxy) and the results are compared. The samples made are as follows (A is a pure and reference sample). It should be noted that other samples including epoxy resin and polyaniline alone with the same percentage composition and epoxy resin and the physical combination of polyaniline and carbon nanotubes in a ratio of 50/50 by weight were also made to conduct electrical conductivity tests.

In order to prepare nanocomposites, for every 100 phr of epoxy resin, 38 phr of curing system is used. The working method is that after weighing the ingredients, the hardener is poured into a 200 ml beaker, then core-shell nanoparticles are added to the beaker. Because the hardener has a lower viscosity than epoxy, the nanoparticles are better dispersed. The mixture is mixed with a shear mixer for 10 minutes. Before the epoxy is added to the hardener/nanotube mixture, we place the epoxy resin at 30-50 °C for 5 minutes to lower its viscosity. After that, the heated resin is added to the mixture and mixed with a shear stirrer for 5 minutes until the epoxy with hardener and nano particles is completely homogenized. During the mixing process, air particles penetrate into the mixture, which, if the part is made without debubble, will create stress concentration points and cause defects in the samples. In order to debubble the mixture, the mixture is placed in a vacuum oven under ambient temperature and pressure of 0.7 bar for 10 minutes. During debubbling, every 2 minutes we take out the sample from the vacuum oven and stir it gently and put it back in the oven so that all the bubbles are removed and the nanoparticles do not settle.

Table 1. Formulations of various prepared epoxy/CNT nanocomposites

Sample code	Type of reinforcement	Weight percent
Epoxy	-	-
Core-shell 1	Core-shell	1
Core-shell 2	Core-shell	2
Core-shell 4	Core-shell	4
CNT 1	Carboxylated CNT	1
CNT 2	Carboxylated CNT	2
CNT 4	Carboxylated CNT	4

2.3 Characterization

Fourier transform infrared (FTIR) spectrometry technique and Bruker Equinox 55 LSI01 FTIR spectrophotometer, Nederland, were used to investigate the type of chemical bonds and functional groups in the chemical structure of the synthesized core-shell nanocomposite. For this purpose, a specific weight of nanoparticles was mixed with dry potassium bromide and a tablet was prepared from that. FTIR spectroscopy of samples in the wavelength range of 400 to 4,000 cm^{-1} was done with 16 scans and sensitivity up to 4 cm^{-1} .

The morphology and microscopic structure of prepared Epoxy/CNT nanocomposites containing various MWCNTs loading was investigated by using cryogenic fracture surfaces of the samples coated with gold and observed using a VegaII XMU scanning electron microscope (SEM), Czech Republic.

Differential scanning calorimetry analysis of all the samples (epoxy nanocomposites containing core-shell nanoparticles and epoxy nanocomposites containing carboxylated carbon nanotubes) was performed by Mettler differential scanning calorimeters (DSC) device, USA. DSC test of the samples under nitrogen atmosphere. The heating rate has been done from ambient temperature to 200 $^{\circ}\text{C}$.

The phase structure of the Epoxy/MWCNTs nanocomposites was investigated by dynamic mechanical thermal analysis (DMTA) using Triton Technology Tritec 2000DMA (UK). Measurements of storage modulus and damping factor were carried out in bending mode at a constant heating rate of 10 $^{\circ}\text{C}/\text{min}$ and a frequency of 1 Hz in a strain of 0.02 mm from 20 $^{\circ}\text{C}$ to roughly 240 $^{\circ}\text{C}$.

Stress-strain behavior of prepared nanocomposites was measured at a cross head speed of 1 mm/min using an Instron 6025 universal testing machine according to ASTM D638.

Electrical conductivity test using the electrical conductivity testing device of the company's product Taiwan Good Will Instrument type LCR-8000G was measured in the frequency range of 20 Hz to 1 MHz and voltage of 1 V. The prepared samples should be disk-shaped with a diameter of 5 cm and a thickness of at least 1 mm.

The output of the mentioned device is the mixed dielectric constant (ϵ_r), which has two elastic (ϵ') and dissipative (ϵ'') components. In fact, the elastic component indicates the permeability of the samples and the dissipation component is related to the dissipation factor D or $\tan\delta$ with the elastic component according to the following relationships:

$$\epsilon_r = \epsilon' - i\epsilon''$$

$$|\epsilon_r| = \sqrt{\epsilon'^2 + \epsilon''^2}$$

$$\epsilon'' = D\epsilon'$$

$$D = \tan \delta$$

$$\varepsilon' = \frac{C\delta}{\varepsilon_0 A} \quad (1)$$

where A is the surface area of the sample which for the prepared disk samples it is equal to 0.000638 m^2 . The thickness of the sample (δ) is in meters and is equal to 0.0026 m . Dielectric constant of vacuum is equal to $8.85 \times 10^{-12} \text{ F/m}$.

To calculate the relationship between the dielectric constant and the concentration of nanoparticles, various theoretical relationships have been presented, which include the dielectric constant of the nanocomposite (ε_c), the dielectric constant of the matrix (ε_m), the dielectric constant of nanoparticles (ε_f), the volume fraction of nanoparticles (φ_f), and the volume fraction of the matrix (φ_m).

$$\text{Bruggman's Formula: } \varepsilon_c = \frac{\varepsilon_m}{(1 - \varphi_f)^3}$$

$$\text{Bottcher's Formula: } \varepsilon_c = \frac{\varepsilon_m}{1 - 3\varphi_f}$$

$$\text{Van Beek's Formula: } \varepsilon_c = \frac{\varepsilon_m(1 + \varphi_f)}{1 - 4\varphi_f}$$

$$\text{Power equation: } \varepsilon_c = \varepsilon_m(1 + \varphi_f)^5 \quad (2)$$

Electrical modulus is a powerful tool for investigating the electrical behavior of polymers and polymer nanocomposites. The complex electric modulus is actually the reciprocal of the complex dielectric constant and can be calculated from the following equation:

$$M_r(\omega) = 1/\varepsilon_r \quad (\omega) = 1/(\varepsilon' - i\varepsilon'')$$

$$M_r(\omega) = M'(\omega) + iM''(\omega)$$

$$= \frac{\varepsilon'}{\varepsilon'^2 + \varepsilon''^2} + i \frac{\varepsilon''}{\varepsilon'^2 + \varepsilon''^2} \quad (3)$$

3. Results and discussion

3.1 FTIR analysis

Figure 1(a) shows the FTIR spectrum of emeraldine salt. In the FTIR spectrum obtained from emeraldine salt powder, five main absorption peaks can be identified in the areas of 788 , $1,117$, $1,292$, $1,477$, $1,560$ and $3,437 \text{ cm}^{-1}$. The absorption peaks observed in the FTIR spectrum of synthesized pure emeraldine salt are in good agreement with previous scientific reports [30, 31]. The absorption peak observed at the frequency of 788 cm^{-1} is related to the out-of-plane bending vibrations of the =C-H bond of the aromatic rings. The broad absorption peak observed at the frequency of $1,117 \text{ cm}^{-1}$ is the peak indicating the presence of conductivity in polyaniline [32]. This absorption peak is related to the stretching vibrations of B-N+H-Q or B-NH-B bonds (B is a benzene ring and Q is a quinonic ring) [33]. The

peak observed at the frequency of $1,292\text{ cm}^{-1}$ is related to aromatic amines (stretching vibrations of C-N bonds) in the chemical structure of polyaniline. Absorptions observed at frequencies of $1,477\text{ cm}^{-1}$ and $1,560\text{ cm}^{-1}$ are related to stretching vibrations of C=C bonds in benzene and quinonic rings, respectively [34]. The intensity ratio of these two peaks can be suitable to determine the oxidation state of the synthesized polyaniline. As seen in Figure 1(a), the intensity of these two peaks are almost equal, which indicates that the synthesized polyaniline chains are mainly in the oxidation state of emeraldine. The broad peak observed in the frequency range of $3,300\text{ cm}^{-1}$ to $3,600\text{ cm}^{-1}$ with peak $3,437\text{ cm}^{-1}$ are related to the stretching vibrations of N-H bonds in the chemical structure of polyaniline [35]. It should be noted that the presence of moisture in the sample can cause the appearance of a broad and elongated absorption peak (corresponding to the stretching vibrations of O-H bonds) in this area and thus interfere with the absorption peak of N-H bonds. Figure 1(b) shows the FTIR spectrum of the synthesized core-shell structure containing 10 wt%, of multi-walled carbon nanotubes. It can be seen that the FTIR peaks of the synthesized nanocomposite are very similar to the FTIR peaks of pure emeraldine salt. The absorption peak observed at the frequency of $1,694\text{ cm}^{-1}$ is related to the out-of-plane bending vibrations of the =C-H bond of the aromatic rings [36]. The broad absorption peak observed at the frequency of $1,123\text{ cm}^{-1}$ is the indicator of the presence of conductivity in polyaniline. This absorption peak is related to the stretching vibrations of B-N+H-Q bonds or B-NH-B, (B is benzene ring and Q is quinone ring) [37]. The peak observed at the frequency of $1,295\text{ cm}^{-1}$ is related to aromatic amines (stretching vibrations of C-N bonds) in the chemical structure of polyaniline [38].

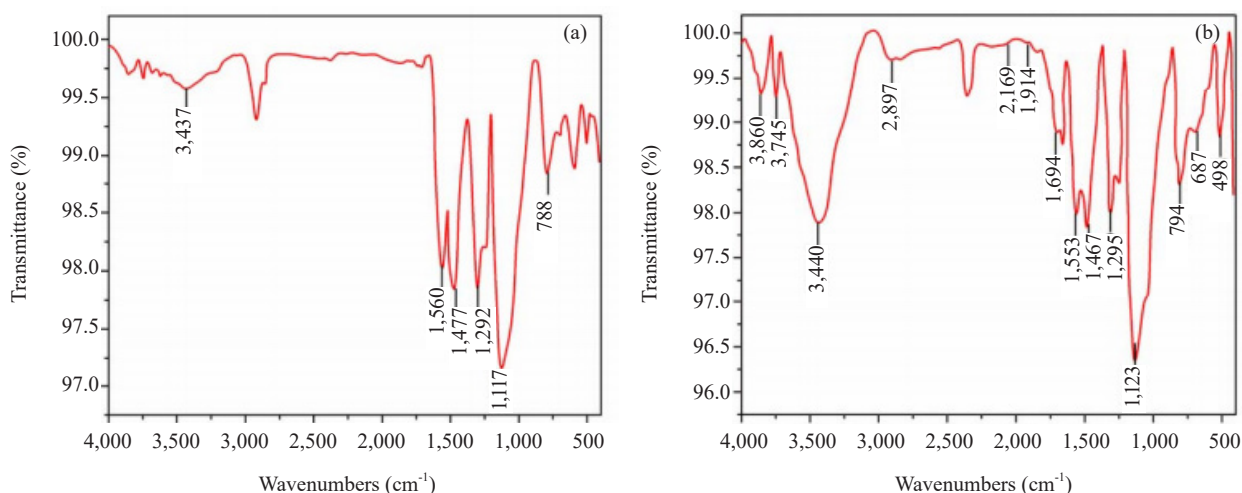


Figure 1. The results of FTIR analysis of (a) Emeraldine salt and (b) synthesized core-shell structure

The peak intensity observed at frequency of $1,467\text{ cm}^{-1}$ (benzoid ring stretching vibration) is almost equal to the peak intensity observed at $1,553\text{ cm}^{-1}$ frequency (C=C stretching vibration of quinoid ring), which indicates that the polyaniline chains in the nanocomposite such as pure polyaniline, it is in the oxidized form of emeraldine. The broad peak observed in the frequency range of $3,300\text{ cm}^{-1}$ to $3,600\text{ cm}^{-1}$ with the peak at $3,440\text{ cm}^{-1}$ is related to the stretching vibrations of the N-H bonds in the chemical structure of polyaniline [38]. It should be noted that the presence of moisture in the sample can cause the appearance of a broad and elongated absorption peak (corresponding to the stretching vibrations of O-H bonds) in this area and thus interfere with the absorption peak of N-H bonds.

3.2 Morphology observations

The SEM image of carboxylated multi-walled carbon nanotubes is represented in Figure 2. In this image, the tubular structure of multi-walled carbon nanotubes can be clearly seen. Using the scale at the bottom of the image, it can be seen that the approximate dimensions of the nanotubes are about 50 nm.

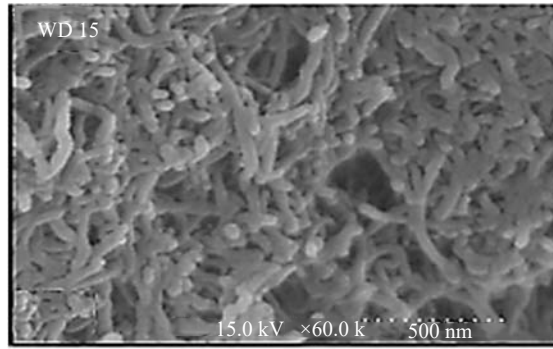


Figure 2. The SEM photomicrograph of carboxylated multi-walled carbon

In Figure 3, SEM images of synthesized nanocomposites with core-shell morphology in the temperature range of 0 to 5 °C and in Figure 4, the SEM images of nanocomposites synthesized in the temperature range of 20 to 25 °C, containing 10% by weight of carboxylated carbon nanotubes are presented. As can be seen, the images obtained from the samples synthesized at a temperature range of 20 to 25 °C have a better tubular morphology and surface than the samples synthesized at a temperature range of 0 to 5 °C, and the synthesised samples at the temperature range of 0 to 5 °C are not tubular and are lumpy. In these images, it can be clearly seen that polyaniline uniformly covers the surface of carbon nanotubes. Therefore, all subsequent samples have been synthesized at a temperature range of 20 to 25 °C to perform various tests.

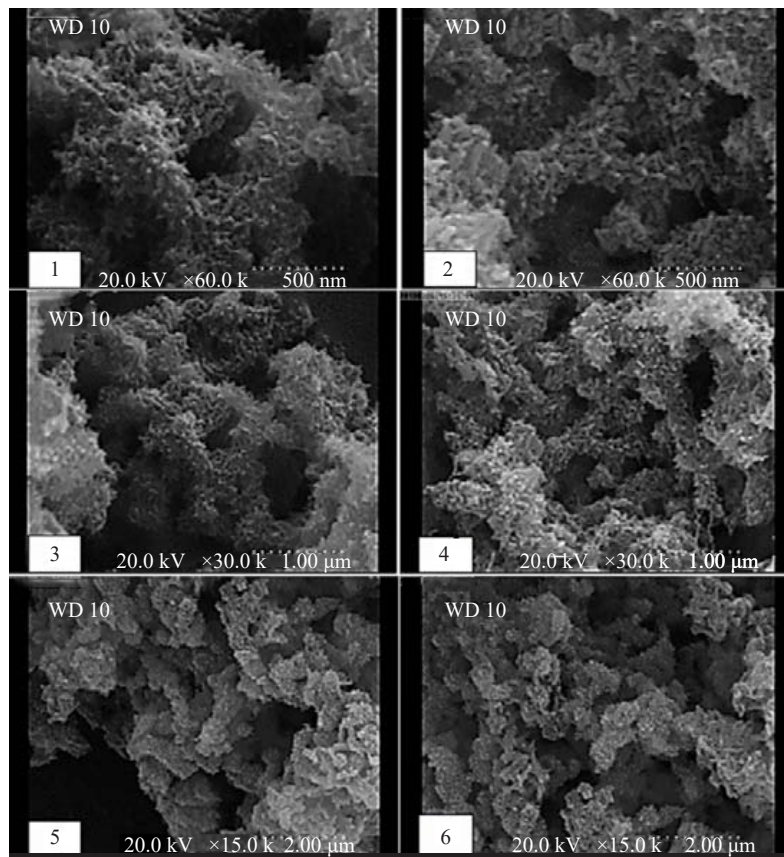


Figure 3. SEM images of synthesized nanocomposites with core-shell morphology in the temperature range of 0 to 5 °C

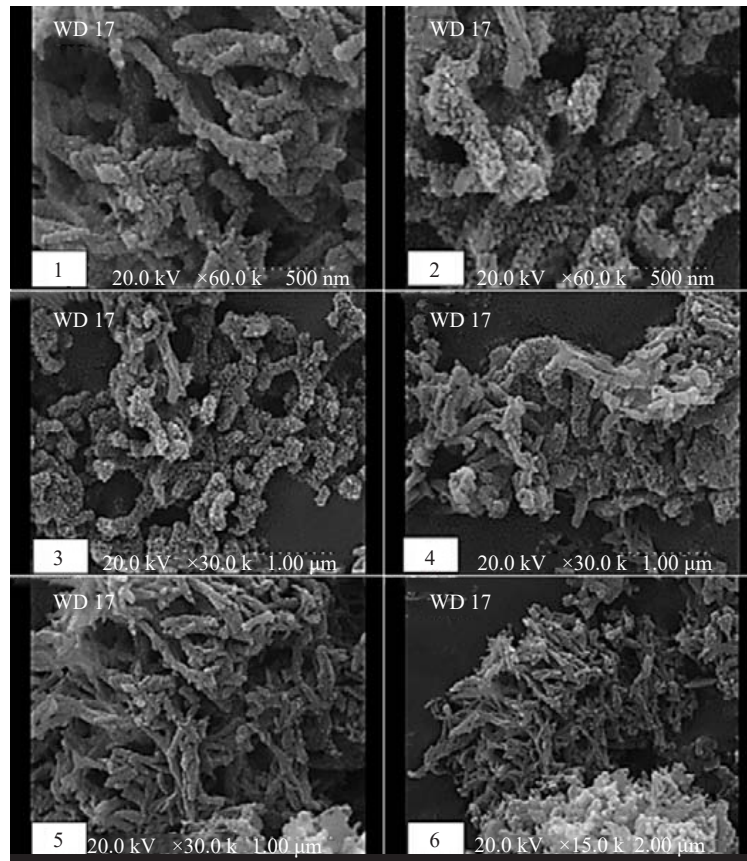


Figure 4. SEM images of synthesized nanocomposites with core-shell morphology in the temperature range of 20 to 25 °C

3.3 DSC analysis

In order to investigate the effect of nanofillers on the curing of the epoxy system, DSC measurements were carried out for all prepared nanocomposites and the results are shown in Table 2. The more reactions that take place in the curing process, the more energy released (curing heat) and the sample will have a lower energy level which leads to more stability.

Table 2. The results of DSC measurements for various epoxy/MWCNTs nanocomposites

Sample code	Initial cure temperature (°C)	Peak temperature (°C)	End cure temperature (°C)	Cure enthalpy (J/gr)
Epoxy	74	140	195	150.2
Core-shell 1	80	138	185	166
Core-shell 2	80	135	180	186.2
Core-shell 4	76	130	190	165
CNT 1	74	130	190	169
CNT 2	74	135	190	162.5
CNT 4	74	135	190	155

According to Table 2, with the addition of C-MWCNTs, the released energy has increased, which indicates more stabilization of the nanocomposite. The core-shell 2 sample has the highest amount of energy released, which indicates that the interface of the core-shell nanoparticles and the resin are well engaged and have released energy. It should be noticed that there is the greatest balance between the amount of N-H functional groups and the baking system in this sample. In the sample of core-shell 4, due to the high amount of nanoparticles (4%), the balance between the amount of N-H functional groups and the curing system has decreased, preventing the complete formation of cross-links and actually preventing the full growth of the links [39]. In the comparison of core-shell 1 and CNT 1 samples, which used 1 wt% of nanoparticles, according to Table 2, the released energy of the samples is equal to 166 and 169 J/g, respectively, and it can be interpreted that the factor the increase in energy released in Core-shell 3 is the interface and interactions between the epoxy resin and the carboxylic groups of nanotubes, which is more than the interactions between the N-H functional groups and the curing system [40]. In the comparison of core-shell 2 and CNT 2 samples, which used 2% of nanoparticles, according to Table 2, the released energy of the samples is equal to 186.2 and 162.5 J/g, respectively, and it can be interpreted as follows showed that the reaction between epoxy and core-shell nanoparticles in the core-shell sample 2 was done very well and was even better than the carbon nanotubes in the CNT 2 sample, and the core-shell sample 2 was the optimal state and there was a good balance between the reactions of the curing system and groups An N-H reaction has taken place [41]. In the comparison of core-shell 4 and CNT 4 samples that used 4% of nanoparticles, according to Table 2, the energy released by the samples is 165 and 155 J/g, respectively, and it can be interpreted that in the percentages above, the polymer interacts better with core-shell nanoparticles than carbon nanotubes. The reason for the increase in the amount of released energy is the reaction of NH groups in the core-shell nanoparticles and the reaction of carboxylic agents in carboxylated nanotubes with epoxy groups [42].

3.4 DMTA measurements

The storage modulus curves in terms of temperature for pure epoxy composite, nanocomposites containing 1, 2 and 4% by weight of PANI/MWCNT core-shell nanoparticles and nanocomposites containing 1, 2 and 4% by weight of carboxylated carbon nanotubes were investigated in Figure 5.

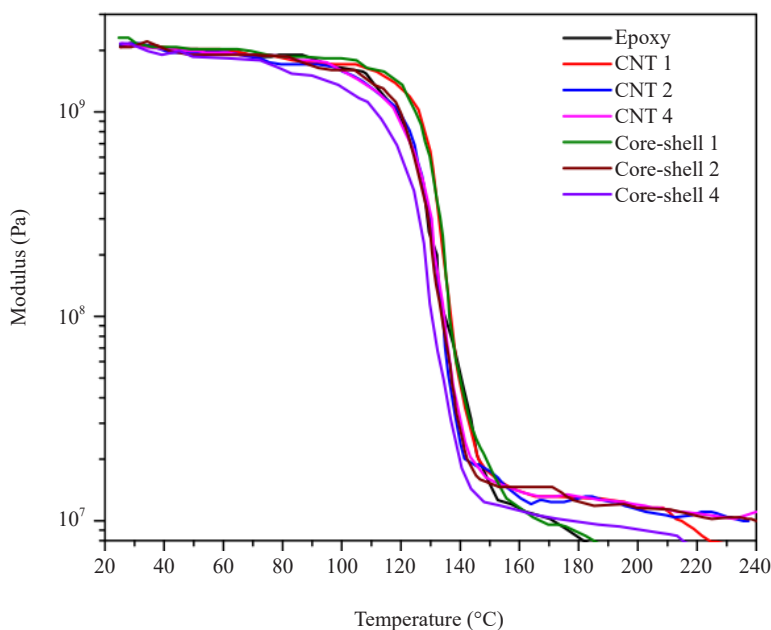


Figure 5. Plots of storage modulus in terms of temperature for prepared epoxy nanocomposites

According to Figure 5, the addition of core-shell nanoparticles and carboxylated nanotubes has a negligible effect on glass-rubber transition temperature (T_g), and this temperature for all samples is in the range of 123 ± 3 °C, which can be attributed to the relatively strong interface between Nanoparticles and epoxy resin attributed. The increase in T_g in the samples containing 1% by weight of nanoparticles is very insignificant, but it can be considered as an increase in thermal stability in these samples, which by reducing the free space between the chains, the movement of the chains has slowed down and has increased the T_g [43]. The decrease in T_g in the samples containing 2 and 4% of nanoparticles is caused by the increase in the free volume in the sample, which is due to the low density of the nanoparticles used [44]. According to Figure 5, Epoxy samples and core-shell 1 have entered the second phase transition at 200 °C, but in other samples, due to the increase in the amount of nanoparticles, the samples become more stable to heat. Figure 6 shows $\tan\delta$ curves in terms of temperature for pure epoxy composite, nanocomposites containing 1, 2 and 4% by weight of PANI/MWCNT core-shell nanoparticles and nanocomposites containing 1, 2 and 4% by weight of carboxylated carbon nanotubes.

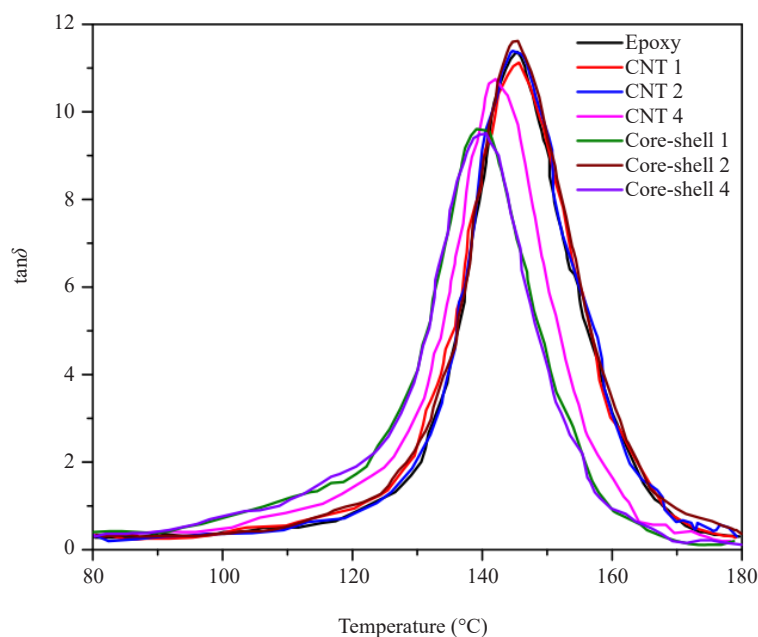


Figure 6. The $\tan\delta$ curves for various epoxy nanocomposites

The wider the area under the loss factor curve, due to the increase of transverse connections, the sample will repel the incoming force to a greater extent and its damping is greater, and the sharper the curve, the more fragile the sample will be. According to Figure 6, the sample containing two percent of core-shell nanoparticles (core-shell sample 2) has the highest area under the curve and has the highest loss, which can be attributed to the balance between the reaction of the N-H groups of polyaniline and the baking system with Epoxy resin is known to make the interface between nanoparticles and resin interact well [45]. The core-shell 4 sample has the lowest area under the curve and the lowest loss. The reason can be explained as follows: by using a high percentage of nanoparticles (4%), the high accumulation of nanoparticles prevented the formation of crosslinks completely and hindered the full growth of the links [46].

3.5 Stress-strain behavior

Figure 7 represents the stress-strain diagrams obtained from the tensile test for all samples. From the stress-strain diagrams, the final stress values, which is the stress at the breaking point, were obtained. For a better comparison and analysis of the results, the values of yield stress, Young's modulus and strain at the breaking point of all samples are given in Table 3.

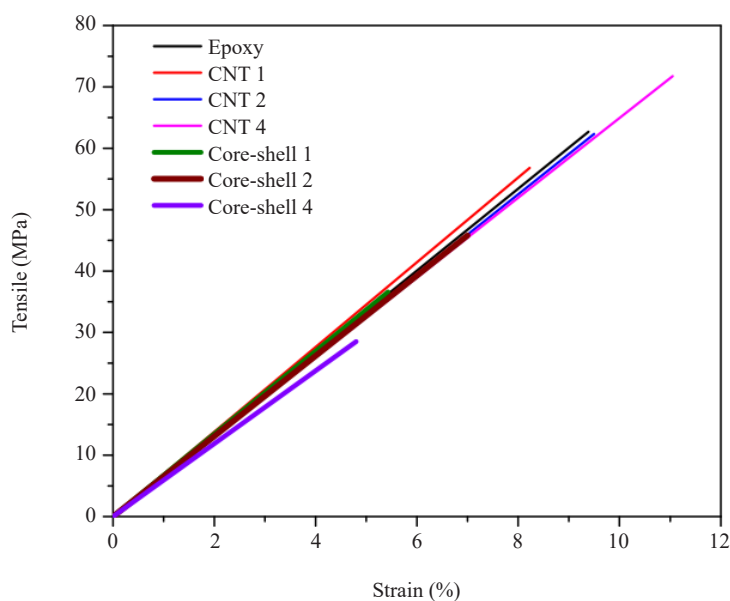


Figure 7. Stress-strain curves of various prepared epoxy/MWCNTs nanocomposites

Table 3. The results of stress-strain behavior for prepared nanocomposites

Sample code	Young's modulus (MPa)	Elongation at break (%)	Tensile strength (MPa)
Epoxy	672	9.4	63.0
Core-shell 1	678	5.4	36.6
Core-shell 2	656	7.0	45.8
Core-shell 4	593	4.8	28.5
CNT 1	685	8.2	56.4
CNT 2	660	9.5	62.5
CNT 4	649	11	71.8

As seen in Table 3, with the increase in the amount of core-shell nanoparticles, the strength of the sample first increases by 2% and then decreases by 4%. It is known that the optimal mode in the use of core-shell nanoparticles is the use of two percent core-shell nanoparticles, the reason for which is the establishment of a proper balance between the reaction of the N-H groups of the nanoparticles with the epoxy resin and the reaction of the curing system with the epoxy resin [47]. According to Table 3, with the increase in the percentage of C-MWCNTs, the tensile strength has increased, which is due to the good compatibility of carboxylated groups on the surface of carbon nanotubes and its reaction with epoxy resin [48].

3.6 Electrical conductivity

Figure 8 shows the logarithmic graphs of real or elastic dielectric constant in terms of frequency for different samples. As can be seen, the dielectric constant decreases with increasing frequency. Meanwhile, for pure epoxy, this drop is very small and the dielectric constant is a constant value at all frequencies except the initial frequencies.

The noteworthy point in this graph is that with the increase of C-MWCNT concentration in epoxy resin, the amount of dielectric constant is increased and a significant difference is observed at the concentration of 4% by weight. However, in the case of nanocomposites containing core-shell particles, no significant change was observed except for 2% by weight, and on the other hand, the dielectric constant of core-shell nanocomposites was lower than that of nanocomposites containing C-MWCNT, and it was close to that of nanocomposite containing 1 weight percent of C-MWCNT are located. It seems that by increasing the interaction of core-shell nanoparticles with epoxy chains, compared to epoxy/C-MWCNTs nanocomposites and creating more restrictions for the movement of polymer chains, the elastic dielectric constant is lower than unmodified samples [49].

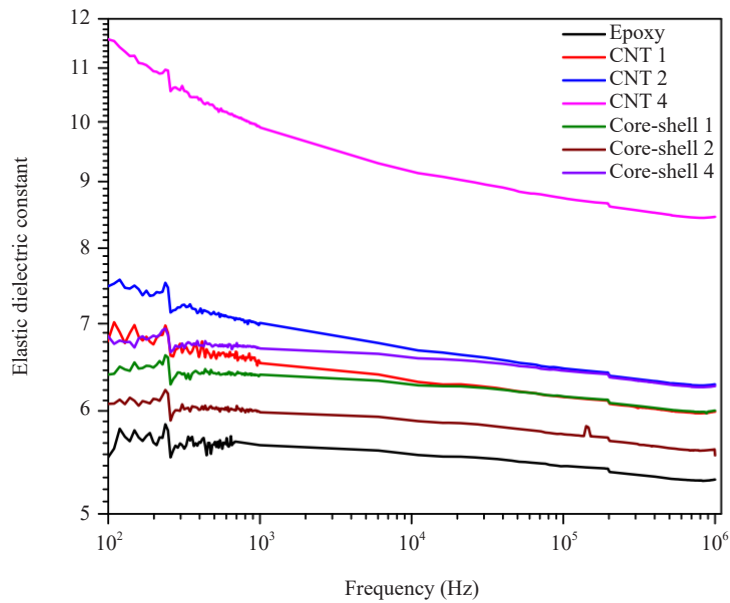


Figure 8. Elastic dielectric constant in terms of frequency for prepared nanocomposites

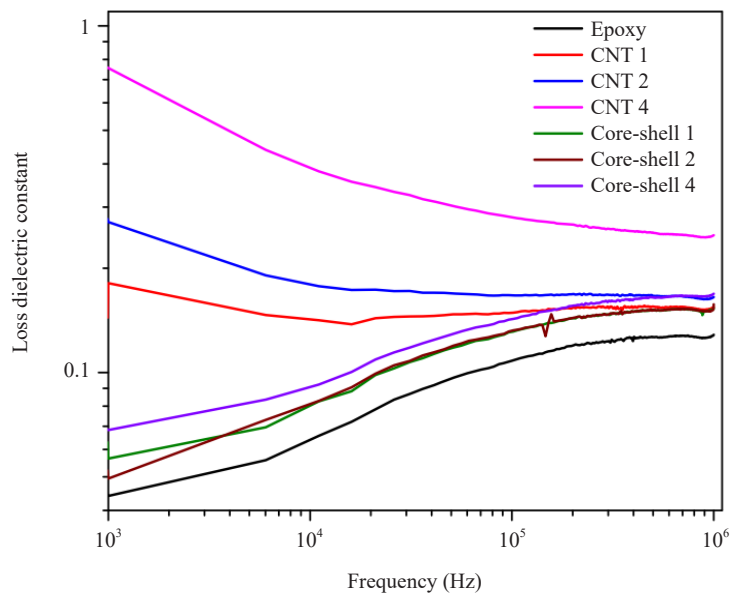


Figure 9. Dissipative dielectric constant variation curve in terms of frequency for prepared nanocomposites

The dissipation dielectric constant diagram for different nanocomposites was demonstrated in Figure 9. The remarkable thing in these graphs is that the process of changes for epoxy resin and core-shell nanocomposites are similar, but CNT nanocomposites show different behavior. According to the graph, it can be seen that the trend of nanocomposites containing CNT, unlike other samples, is uniformly decreasing, but epoxy resin and core-shell nanocomposites first show a decreasing trend, then an increasing trend. It seems that by increasing the amount of interaction between the matrix and the nanoparticles, the constant behavior of the dissipative dielectric moves more towards the pure epoxy resin [50].

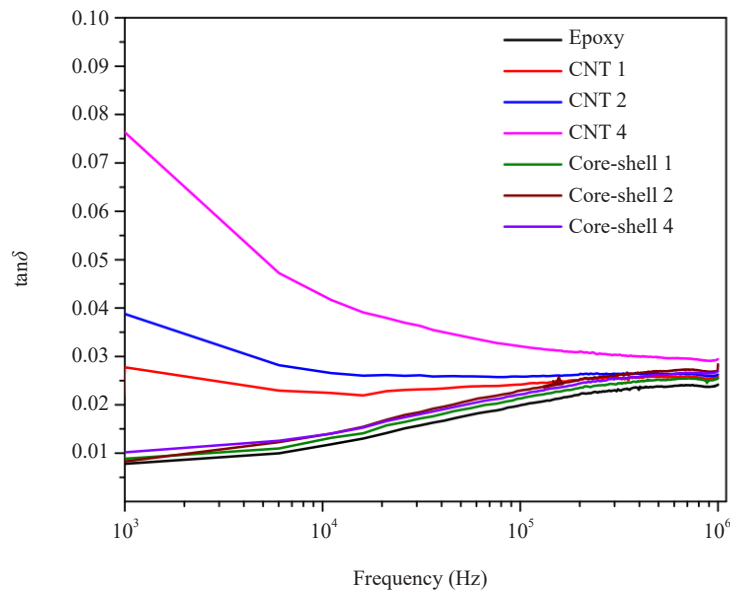


Figure 10. The curve of changes in the electrical dissipation factor in terms of frequency for the prepared nanocomposites

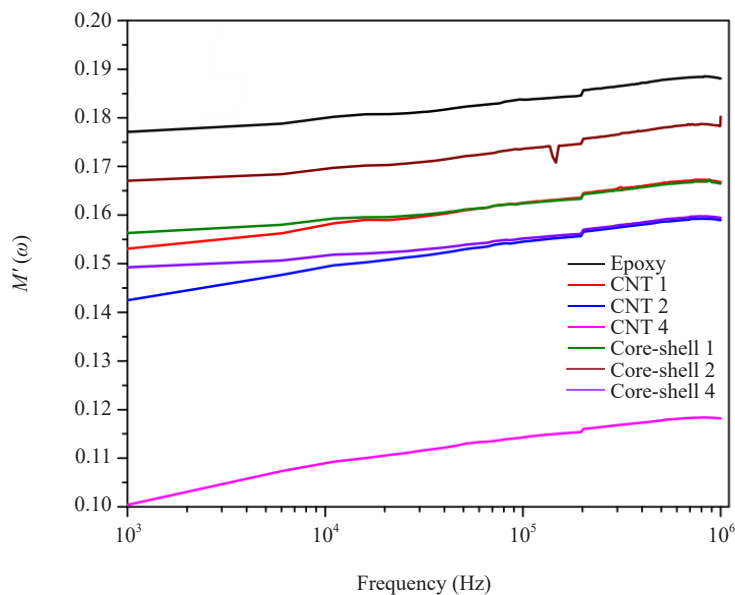


Figure 11. Changes in electrical modulus with different concentrations of carbon nanotubes and core-shell nanoparticles

Figure 10 shows the dielectric loss coefficient of epoxy resin containing carbon nanotubes and core-shell particles. As can be seen in this graph, the increase in dielectric loss coefficient by core-shell particles is lower than C-MWCNT and this behavior can be due to the decrease in the conductivity performance of carbon nanotubes in core-shell structures.

The changes in electrical modulus in terms of frequency for different percentages of carbon nanotubes and core-shell nanoparticles were investigated in Figure 11. As can be seen in this diagram, nanocomposites containing 4% by weight of carboxylated nanotube carbon have the lowest electrical modulus or, in fact, the lowest current resistance. Also, in the case of core-shell nanoparticles, the lowest electrical resistance is observed at 4% by weight. However, the graph shows that the electrical modulus of epoxy nanocomposites/core-shell nanoparticles is in the range of epoxy/carbon nanotube carboxylated nanocomposites with 1 and 2% by weight.

Figure 12 shows the changes in electrical conductivity of different nanocomposites. As can be seen, with the increase of nano reinforcements and the addition of dissipation mechanisms, especially in the interface, the amount of electrical conductivity increases and is maximum for CNT 4. Another point is that with the increase in frequency, the electrical conductivity of all samples increases and approaches each other. This phenomenon shows the greater effect of frequency in increasing electrical conductivity compared to nano amplifiers and is caused by the removal of mechanisms that were added to epoxy resin at low frequencies.

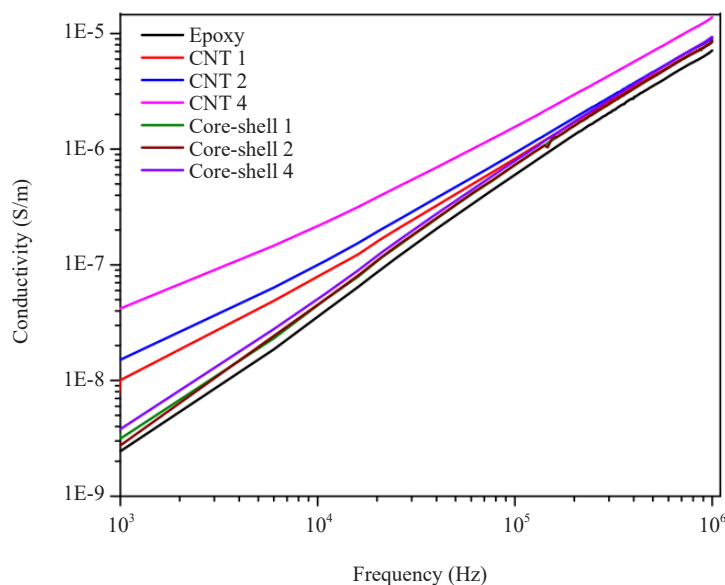


Figure 12. Electrical conductivity changes with different concentrations of carbon nanotubes and core-shell nanoparticles

Figure 13 represents the changes of elastic dielectric constant in terms of volume concentration of nanoparticles in three selected frequencies of 100 Hz, 100 kHz and 1 MHz. In this diagram, Bruggman's equation is used to calculate the dielectric constant. As can be seen, the model results differ greatly from the experimental results, especially for epoxy/carbon nanotube nanocomposites, and the difference increases with increasing nanofiller concentration. But for epoxy nanocomposites/core-shell nanoparticles, this difference is less, and especially in the concentration of 2% by weight, it is in good agreement with the model results.

Figure 14 shows the comparison of Bottcher's model with experimental results. As can be seen, the experimental results related to epoxy/carbon nanotube nanocomposites differ greatly from the theoretical results, but in the case of core-shell nanoparticles, there is a good agreement, especially at high frequencies, i.e. 1 MHz.

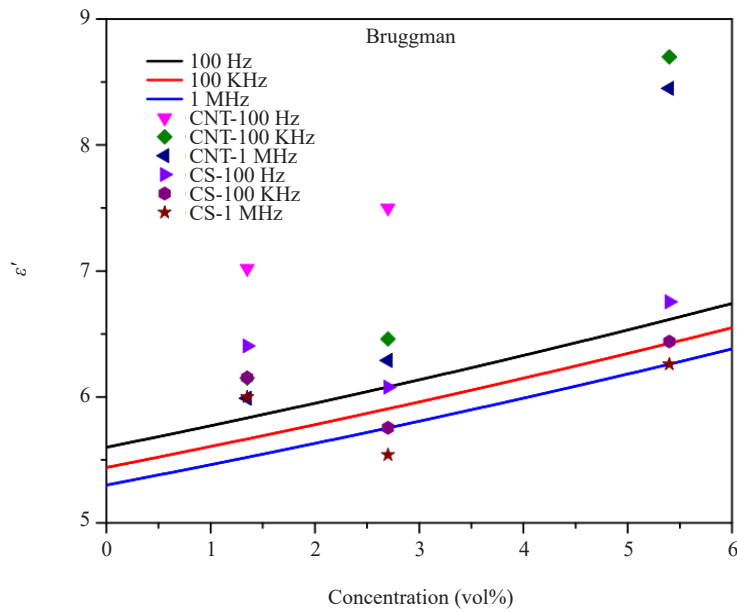


Figure 13. Comparison of Bruggman model results with experimental results for different prepared nanocomposites

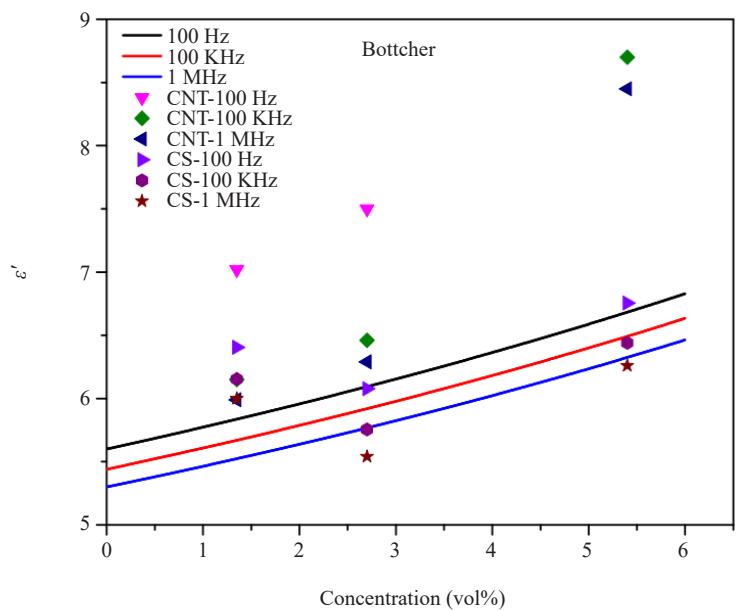


Figure 14. Comparison of Bottcher model results with experimental results for different prepared nanocomposites

Figure 15 also compares the experimental results with Van Beek's model. It seems that this model has less difference with the experimental results, especially in the case of epoxy/carbon nanotube nanocomposites and at high frequencies.

Figure 16 compares the power or Baziard model with the experimental results. As can be seen, the results of this model have less difference from the experimental results compared to the previous models, but with the increase of carbon nanotube concentration, the difference in the results increases. It seems that the models presented above are suitable for micro composites, and better and more complex models should be provided to examine nanocomposites.

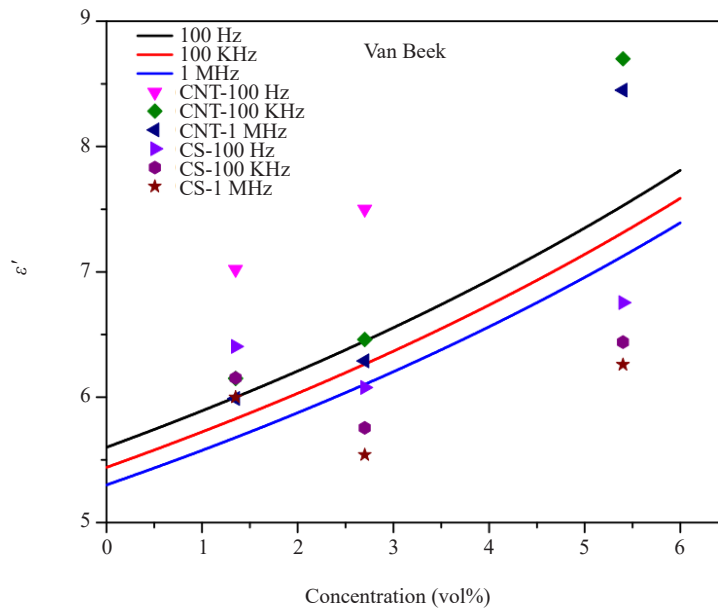


Figure 15. Comparison of Van Beek model results with experimental results for different prepared nanocomposites

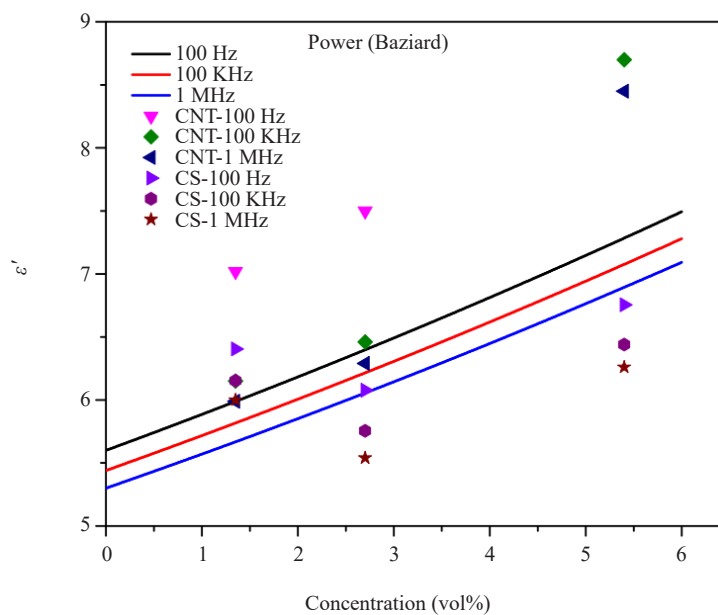


Figure 16. Comparison of power model results with experimental results for different prepared nanocomposites

4. Conclusions

The epoxy nanocomposites containing various concentrations of carboxylated carbon nanotubes (C-MWCNTs) and surface modified C-MWCNTs with polyaniline were prepared and their various properties were investigated. The results of FTIR spectrum revealed that the polyaniline and C-MWCNTs produced a core/shell structure and the SEM images proofed the surface modification of C-MWCNTs. The results of morphological observations show that the diameter of synthesized core/shell nanoparticle was about 200 nm which is higher in comparison to neat C-MWCNTs as identified

about 50 nm in average diameter.

The results of DMTA measurements indicated that by adding core-shell reinforcing nanoparticles and C-MWCNTs to epoxy resin, the glass transition temperature has changed slightly and this temperature is in the range of 123 ± 3 °C for all prepared nanocomposites.

According to the graphs obtained from the DMTA test, the thermal stability has increased in samples containing 2% by weight of core-shell nanoparticles and in all samples containing carboxylated carbon nanotubes.

The sample containing 2 wt%, of core-shell nanoparticles has the largest area under the $\tan\delta$ curve and has the largest loss, which is due to the creation of a strong interface caused by the reaction of the N-H group of polyaniline with epoxy resin. The results of DSC tests show that the addition of core-shell nanoparticles and carboxylated carbon nanotubes did not have much effect on the curing of epoxy resin and it is not needed to change the curing system for nanocomposites. The increase in the energy released during the DSC test in all the samples indicated the higher stabilization of the nanocomposite. Tensile strength decreased in samples containing core-shell nanoparticles and increased in samples containing carboxylated carbon nanotubes, which can be attributed to the compatibility and good reaction of carboxylated groups on the surface of carbon nanotubes with epoxy resin. The results of the electrical conductivity test show that the dielectric constant increased with increasing nanoparticle concentration and decreases with increasing frequency. This drop occurred faster at higher concentrations, especially for nanocomposites containing 4 wt%, of carbon nanotubes. However in the case of nanocomposites containing core-shell nanoparticles in all concentration ranges, a similar trend is observed in the decrease of dielectric constant with frequency change.

Conflict of interest

The author declares no competing financial interest.

References

- [1] Paran SMR, Naderi G, Ghoreishy MHR. XNBR-grafted halloysite nanotube core-shell as a potential compatibilizer for immiscible polymer systems. *Applied Surface Science*. 2016; 382: 63-72.
- [2] Ghosh Chaudhuri R, Paria S. Core/shell nanoparticles: classes, properties, synthesis mechanisms, characterization, and applications. *Chemical Reviews*. 2012; 112(4): 2373-2433.
- [3] Wei S, Wang Q, Zhu J, Sun L, Lin H, Guo Z. Multifunctional composite core-shell nanoparticles. *Nanoscale*. 2011; 3(11): 4474-4502.
- [4] Dai H. Carbon nanotubes: opportunities and challenges. *Surface Science*. 2002; 500(1-3): 218-241.
- [5] Paran SMR, Das A, Khonakdar HA, Naderpour N, Heinrich G, Saeb MR. Modeling and interpreting large deformation behavior of rubber nanocomposites containing carbon nanotubes and nanoplatelets. *Polymer Composites*. 2019; 40(S2): E1548-E1558.
- [6] Lyons PE, De S, Blighe F, Nicolosi V, Pereira LFC, Ferreira MS, et al. The relationship between network morphology and conductivity in nanotube films. *Journal of Applied Physics*. 2008; 104(4): 044302.
- [7] Piao Y, Tondare VN, Davis CS, Gorham JM, Petersen EJ, Gilman JW, et al. Comparative study of multiwall carbon nanotube nanocomposites by Raman, SEM, and XPS measurement techniques. *Composites Science and Technology*. 2021; 208: 108753.
- [8] Lin PS, Lin JM, Tung SH, Higashihara T, Liu CL. Synergistic Interactions in sequential process doping of polymer/single-walled carbon nanotube nanocomposites for enhanced n-type thermoelectric performance. *Small*. 2024; 20(9): 2306166.
- [9] Paran SMR, Naderi G, Babakhani A. An experimental study of the effect of CNTs on the mechanical properties of CNTs/NR/EPDM nanocomposite. *Polymer Composites*. 2018; 39(11): 4071-4079.
- [10] Paran SMR, Sahraeian R, Naderi G, Rashidi A. Nonlinear elastoplastic behavior induced by multiwalled carbon nanotubes in the compatibilized low density polyethylene/poly (methyl hydrogen siloxane)-grafted perlite nanocomposites. *Mechanics of Materials*. 2019; 136: 103066.
- [11] Beygisangchin M, Baghdadi AH, Kamarudin SK, Rashid SA, Jakmunee J, Shaari N. Recent progress in polyaniline and its composites; Synthesis, properties, and applications. *European Polymer Journal*. 2024; 210: 112948.

- [12] Majeed AH, Mohammed LA, Hammoodi OG, Sehgal S, Alheety MA, Saxena KK, et al. A review on polyaniline: synthesis, properties, nanocomposites, and electrochemical applications. *International Journal of Polymer Science*. 2022; 2022(1): 9047554.
- [13] Gao F, Mu J, Bi Z, Wang S, Li Z. Recent advances of polyaniline composites in anticorrosive coatings: A review. *Progress in Organic Coatings*. 2021; 151: 106071.
- [14] Babel V, Hiran BL. A review on polyaniline composites: Synthesis, characterization, and applications. *Polymer Composites*. 2021; 42(7): 3142-3157.
- [15] Xu H, Cui L, Pan X, An Y, Jin X. Carboxymethylcellulose-polyaniline/carbon nanotube (CMC-PANI/CNT) film as flexible and highly electrochemical active electrode for supercapacitors. *International Journal of Biological Macromolecules*. 2022; 219: 1135-1145.
- [16] Karami Z, Paran SMR, Vijayan PP, Ganjali MR, Jouyandeh M, Esmaceli A, et al. A comparative study on cure kinetics of layered double hydroxide (LDH)/epoxy Nanocomposites. *Journal of Composites Science*. 2020; 4(3): 111.
- [17] Jouyandeh M, Paran SMR, Khadem SSM, Ganjali MR, Akbari V, Vahabi H, et al. Nonisothermal cure kinetics of epoxy/ $MnxFe_{3-x}O_4$ nanocomposites. *Progress in Organic Coatings*. 2020; 140: 105505.
- [18] Jouyandeh M, Akbari V, Paran SMR, Livi S, Lins L, Vahabi H, et al. Epoxy/ionic liquid-modified mica nanocomposites: network formation-network degradation correlation. *Nanomaterials*. 2021; 11(8): 1990.
- [19] Seidi F, Jouyandeh M, Akbari V, Paran SMR, Livi S, Ducos F, et al. Super-crosslinked ionic liquid-intercalated montmorillonite/epoxy nanocomposites: Cure kinetics, viscoelastic behavior and thermal degradation mechanism. *Polymer Engineering & Science*. 2020; 60(8): 1940-1957.
- [20] Akbari V, Jouyandeh M, Paran SMR, Ganjali MR, Abdollahi H, Vahabi H, et al. Effect of surface treatment of halloysite nanotubes (HNTs) on the kinetics of epoxy resin cure with amines. *Polymers*. 2020; 12(4): 930.
- [21] Jouyandeh M, Ganjali MR, Ali JA, Aghazadeh M, Paran SMR, Naderi G, et al. Curing epoxy with polyvinylpyrrolidone (PVP) surface-functionalized $ZnxFe_{3-x}O_4$ magnetic nanoparticles. *Progress in Organic Coatings*. 2019; 136: 105227.
- [22] Paran SMR, Vahabi H, Jouyandeh M, Ducos F, Formela K, Saeb MR. Thermal decomposition kinetics of dynamically vulcanized polyamide 6-acrylonitrile butadiene rubber-halloysite nanotube nanocomposites. *Journal of Applied Polymer Science*. 2019; 136(20): 47483.
- [23] Babahan-Bircan I, Demirkaya I, Hasan SOH, Thomas J, Soucek MD. Comparison of new bio-based epoxide-amine coatings with their nanocomposite coating derivatives (graphene, CNT, and fullerene) as replacements for BPA. *Progress in Organic Coatings*. 2022; 165: 106714.
- [24] Anvari A. The influence of CNT structural parameters on the properties of CNT and CNT-reinforced epoxy. *International Journal of Aerospace Engineering*. 2020; 2020(1): 4873426.
- [25] Zhang D, Huang Y, Chia L. Effects of carbon nanotube (CNT) geometries on the dispersion characterizations and adhesion properties of CNT reinforced epoxy composites. *Composite Structures*. 2022; 296: 115942.
- [26] Shin H. Multiscale model to predict fracture toughness of CNT/epoxy nanocomposites. *Composite Structures*. 2021; 272: 114236.
- [27] Song X, Gao J, Zheng N, Zhou H, Mai Y-W. Interlaminar toughening in carbon fiber/epoxy composites interleaved with CNT-decorated polycaprolactone nanofibers. *Composites Communications*. 2021; 24: 100622.
- [28] Chen X, Peng F, Wang C, Zhou H, Lin X, Liu W, et al. Improving the flame retardancy and mechanical properties of epoxy composites significantly with a low-loading CNT-based hierarchical hybrid decorated with reactive hyperbranched polyphosphoramidate. *Applied Surface Science*. 2022; 576: 151765.
- [29] Merneedi A, Natrayan L, Kaliappan S, Veeman D, Angalaeswari S, Srinivas C, et al. Experimental investigation on mechanical properties of carbon nanotube-reinforced epoxy composites for automobile application. *Journal of Nanomaterials*. 2021; 2021(1): 4937059.
- [30] Cochet M, Louarn G, Quillard S, Buisson J, Lefrant S. Theoretical and experimental vibrational study of emeraldine in salt form. Part II. *Journal of Raman Spectroscopy*. 2000; 31(12): 1041-1049.
- [31] Focke WW, Wnek GE. Conduction mechanisms in polyaniline (emeraldine salt). *Journal of Electroanalytical Chemistry and Interfacial Electrochemistry*. 1988; 256(2): 343-352.
- [32] Chaudhari H, Kelkar D. Investigation of structure and electrical conductivity in doped polyaniline. *Polymer International*. 1997; 42(4): 380-384.
- [33] Bhadra S, Chattopadhyay S, Singha NK, Khastgir D. Improvement of conductivity of electrochemically synthesized polyaniline. *Journal of Applied Polymer Science*. 2008; 108(1): 57-64.
- [34] Zhao X, Imahori H, Zhan C-G, Sakata Y, Iwata S, Kitagawa T. Resonance raman and FTIR spectra of isotope-

- labeled reduced 1,4-benzoquinone and its protonated forms in solutions. *The Journal of Physical Chemistry A*. 1997; 101(4): 622-631.
- [35] Furukawa Y, Ueda F, Hyodo Y, Harada I, Nakajima T, Kawagoe T. Vibrational spectra and structure of polyaniline. *Macromolecules*. 1988; 21(5): 1297-1305.
- [36] Tsuzuki S. Interactions with aromatic rings. *Intermolecular Forces and Clusters I*. Berlin, Heidelberg: Springer; 2005. p.149-193.
- [37] Cao Y, Li S, Xue Z, Guo D. Spectroscopic and electrical characterization of some aniline oligomers and polyaniline. *Synthetic Metals*. 1986; 16(3): 305-315.
- [38] Jaymand M. Recent progress in chemical modification of polyaniline. *Progress in Polymer Science*. 2013; 38(9): 1287-1306.
- [39] Souto LFC, Soares BG. Polyaniline/carbon nanotube hybrids modified with ionic liquids as anticorrosive additive in epoxy coatings. *Progress in Organic Coatings*. 2020; 143: 105598.
- [40] Souto LFC, Henriques RR, Soares BG. Influence of acidic and alkaline environmental anticorrosive performance of epoxy coatings based on polyaniline/carbon nanotube hybrids modified with ionic liquid. *Progress in Organic Coatings*. 2022; 173: 107206.
- [41] Tarawneh MA, Sarairoh SA, Chen RS, Ahmad SH, Al-Tarawni MA, Yu LJ, et al. Mechanical reinforcement with enhanced electrical and heat conduction of epoxy resin by polyaniline and graphene nanoplatelets. *Nanotechnology Reviews*. 2020; 9(1): 1550-1561.
- [42] Xia Z, Wang R, Qu B, Wu Q, Zhuo D, Zheng Y. Microwave absorbing properties of polyaniline coated Buckypaper reinforced epoxy resin composites. *Journal of Applied Polymer Science*. 2022; 139(46): e53154.
- [43] Paran SMR, Naderi G, Javadi F, Shemshadi R, Saeb MR. Experimental and theoretical analyses on mechanical properties and stiffness of hybrid graphene/graphene oxide reinforced EPDM/NBR nanocomposites. *Materials Today Communications*. 2020; 22: 100763.
- [44] Paran SMR, Naderi G, Mirzaee M, Ghoreishy MHR, Włoch M, Esmaeili A, et al. Microstructure-properties relationship in ethylene-propylene diene monomer (EPDM)/nitrile butadiene rubber (NBR)/halloysite nanotubes (HNTs) nanocomposites. *Polymer Bulletin*. 2024; 81(1): 755-772.
- [45] Javaid A, Khalid O, Shakeel A, Noreen S. Multifunctional structural supercapacitors based on polyaniline deposited carbon fiber reinforced epoxy composites. *Journal of Energy Storage*. 2021; 33: 102168.
- [46] Zhang J, Zhu A. Study on the synthesis of PANI/CNT nanocomposite and its anticorrosion mechanism in waterborne coatings. *Progress in Organic Coatings*. 2021; 159: 106447.
- [47] Rahnamol AM, Gopalakrishnan J. Improved dielectric and dynamic mechanical properties of epoxy/polyaniline nanorod/in situ reduced graphene oxide hybrid nanocomposites. *Polymer Composites*. 2020; 41(8): 2998-3013.
- [48] Tan W, Stallard JC, Jo C, De Volder MF, Fleck NA. The mechanical and electrochemical properties of polyaniline-coated carbon nanotube mat. *Journal of Energy Storage*. 2021; 41: 102757.
- [49] Rashid IA, Tariq A, Shakir HF, Afzal A, Ali F, Abuzar M, et al. Electrically conductive epoxy/polyaniline composite fabrication and characterization for electronic applications. *Journal of Reinforced Plastics and Composites*. 2022; 41(1-2): 34-45.
- [50] Rashidifard S, Amraei IA, Heidar H, Mousavi SR. Investigating the electrical properties of epoxy resin containing MWCNT-PANI with a core-shell morphology: synthesis and characterization. *Polymer Science, Series B*. 2021; 63(4): 418-431.